# Shaking Table Test on Mitigation of Liquefaction-Induced Tunnel Uplift by Helical Pile

Nokande, Saber; Haddad, Abdolhosein; Jafarian, Yaser

**DOI**
10.1061/(ASCE)GM.1943-5622.0002607

**Publication date**
2022

**Document Version**
Final published version

**Published in**
International Journal of Geomechanics

**Citation (APA)**
Nokande, S., Haddad, A., & Jafarian, Y. (2022). Shaking Table Test on Mitigation of Liquefaction-Induced Tunnel Uplift by Helical Pile. *International Journal of Geomechanics*, *23*(1), Article 04022243. https://doi.org/10.1061/(ASCE)GM.1943-5622.0002607

# Shaking Table Test on Mitigation of Liquefaction-Induced Tunnel Uplift by Helical Pile

Saber Nokande[1]; Abdolhosein Haddad[2]; and Yaser Jafarian[3]

**Abstract:** The tunnels located in the shallow depths of loose saturated sand are significantly prone to liquefaction-induced uplift. Research works are, therefore, in progress to propose efficient techniques for mitigating uplift. In this study, 1 g physical modeling was used to assess the performance of helical piles for decreasing liquefaction-induced uplift. The effects of pile length, number of pile helixes, and the pile spacing in plan view were investigated. The uplift mechanism of the tunnel and helical pile system was also analyzed. The results demonstrate that the penetration of the helical piles into the dense layer underlying the superficial liquefiable sand has decreased tunnel uplift significantly. However, excessive close pile spacing along the tunnel resulted in shear surface interference, and the efficiency of the excessive number of helical piles decreased significantly. The detailed view of the uplift mechanism showed that utilization of the piles extended the transition phase of uplift during shaking. Helical piles can efficiently restrict the possibility of rapid uplift of the tunnel and shorten the duration of the primary uplift phase. **DOI: 10.1061/(ASCE)GM.1943-5622.0002607**. © *2022 American Society of Civil Engineers*.

**Author keywords:** Liquefaction; Tunnel; Uplift mechanism; Helical pile; Shaking table.



## Introduction

Different types of underground structures, including pipelines, chambers, manholes, and subways, are used in cities. The liquefaction phenomenon, which causes uplift in shallow underground structures, is dangerous for buried structures located in loose saturated sandy soils. The evidence of uplifted underground structures induced by soil liquefaction was observed in numerous earthquakes, such as the 1964 Niigata Earthquake and the 1983 Nihonkai-Chubu Earthquake (Kitaura and Miyajima 1988), the Chi-Chi Earthquake of 1999 in Taiwan (Chen et al. 2000), the 2004–2007 Niigata Earthquakes (Tobita et al. 2009), and the 2011 Tohoku Earthquake (Chian and Tokimatsu 2012). Hence, it is vital to identify the liquefaction-prone areas for proper design. For example, the study by Nath et al. (2022) examined the liquefaction potential of the densely populated region of West Bengal with an emphasis on its capital city, Kolkata.

Liquefaction-induced uplift in underground structures has been of great interest to researchers in recent years because such structures are critical to daily life. The importance of liquefaction-induced uplift in the underground structures led to research on the uplift mechanism such as the studies by Kosekt et al. (1997) and Stringer and Madabhushi (2007) through shaking table tests; Chian and Madabhushi (2012), Chou et al. (2011), and Ling et al. (2003) using centrifuge tests; and Castiglia et al. (2018), Ling et al. (2008), Liu and Song (2005), and Sudevan et al. (2018, 2020a) with numerical studies. Chian et al. (2014) revealed that the displacement of liquefied soil around the displaced circular structure resembled a global circular flow mechanism from the top of the underground structure to its bottom. The soil around the rectangular construction, on the other hand, exhibited a distinct mechanism in which the displacement resembled a flow mechanism from two sides of the structure to its bottom (Bao et al. 2017). Zheng et al. (2021) numerically investigated the uplift mechanism of twin underground structures with different spacing. Two nearby tunnels produced less uplift than a single tunnel, but the uplift steadily increased with spacing to approximate the single tunnel uplift. Despite the observed damage from liquefaction of numerous underground structures in previous seismic events, researchers investigated several methods of mitigating structural displacement.

The densification method is one of the traditional techniques to prevent liquefaction examined by Modoni et al. (2018), Olarte et al. (2018), and Mele et al. (2019). In this method, compaction helps to restrict the pore water movement in the improved region. The required densified area was proposed in the design procedure by Tanaka et al. (1995) based on their experimental studies. In addition, Tobita et al. (2011) studied the effect of the soil relative density and reported that the loose sand caused more uplift displacement in large underground structures.

Adalier et al. (2003), Orense et al. (2003), Otsubo et al. (2016a, b), and Paramasivam et al. (2018) investigated the effect of excess porewater pressure (EPWP) dissipating from the vicinity of the structure. Accordingly, dewatering (Yegian et al. 2007; Mitsuji 2008) can reduce the liquefaction effects. Miyajima et al. (1992), Orense et al. (2003), Yang et al. (2004), Otsubo et al. (2016b), and Mahmoud et al. (2020) used drainage systems around the underground structures by replacing the liquefiable soil with permeable soil. However, dissipating the EPWP is not the only way, and using cutoff walls and barriers around the structures to restrict the lateral flow of the soil near the pipeline and tunnel is another method for mitigating the liquefaction-induced uplift (Yoshimi 1998; Yasuda and Kiku 2006; Liu and Song 2006). Some other methods, such as placing weights above the pipelines (Taeseri et al. 2016; Castiglia et al. 2017) or placing geogrids in the overlying soil (Castiglia et al. 2019), reduced the liquefaction-induced uplift of buried pipeline structure.

[1]Ph.D. Candidate, Dept. of Civil Engineering, Semnan Univ., P.O. Box 35131–19111, Semnan, Iran. Email: snokande@semnan.ac.ir

[2]Associate Professor, Dept. of Civil Engineering, Semnan Univ., P.O. Box 35131–19111, Semnan, Iran (corresponding author). Email: haddad@semnan.ac.ir

[3]Associate Professor, Geotechnical Engineering Research Center, International Institute of Earthquake Engineering and Seismology (IIEES), P.O. Box 19395–3913, Tehran, Iran; Research Fellow, Delft Univ. of Technology, Mekelweg 5, 2628 CD Delft, Netherlands. ORCID: https://orcid.org/0000-0001-9741-5461. Email: yjafarianm@iiees.ac.ir

Note. This manuscript was submitted on February 4, 2022; approved on July 15, 2022; published online on October 20, 2022. Discussion period open until March 20, 2023; separate discussions must be submitted for individual papers. This paper is part of the ***International Journal of Geomechanics***, © ASCE, ISSN 1532-3641.

Some of the studies use a combination of mitigation methods, such as the densified wall and gravel drain on both sides of the structure (Adalier et al. 2003), which exhibited promising results in reducing the uplift. Further, Mahmoud et al. (2020) found that the combined use of an impermeable layer under the structure and gravel drains on the sides of the tunnel effectively reduced the liquefaction-induced uplift of the tunnel. According to Sudevan et al. (2020b), the performance of discontinuous replacement with intervals equal to the tunnel diameter was comparable to that of continuous replacement of the same width. Otsubo et al. (2016b) used various recyclable materials to mitigate the uplift displacement of pipelines placed in liquefiable soil. They reported that crushed glass was the most effective of the selected materials due to its higher permeability.

Utilizing these techniques is costly when used for long-track structures. Additionally, some methods need massive excavation or cannot be performed after construction of a pipeline or tunnel. Sometimes equipment might have space constraints or generate a lot of noise and vibration, making these approaches inappropriate for utilization in urban environments. Nevertheless, using helical piles in the invert of tunnels has many positive aspects. The advantages of the helical pile method include the resistance of helical piles to the uplift effects of the tunnels due to their high tensile capacities, suitability for installation sites with limited space or access inside the tunnels, and low disturbance to the surrounding soil.

The enormous overturning moments induced by lateral loads often affect the design of tall and light buildings such as wind turbines, latticed towers (i.e., supporting telecommunication equipment), and light-gauge steel frame structures. These structures are often more challenging to withstand tension loads than compression loads due to the moments that generate tension–compression force couples, which expose windward side foundations to high net uplift forces. Due to the high tensile capacity of helical piles, utilizing this type of pile is increasingly being employed in practice to withstand the uplift effects of lateral stresses (Mohajerani et al. 2016; Perko 2009). Many researchers investigated the uplift capacity of the helical piles. Generally, the uplift capacity of the helical piles is simplified as a circular plate due to the similar mechanism of helical piles under tension loads, and most previous studies were conducted experimentally. The main uplifting experiments were conducted using 1 g table tests by Das and Seeley (1975), Murray and Geddes (1987), Sutherland (1988), Ilamparuthi et al. (2002), and Liu et al. (2012) and a centrifuge table test by Dickin (1988) and Tagaya et al. (1988).

According to the previous studies on the acceptable performance of the helical pile in uplift resisting (Sharma and Guner 2020; Guner and Chiluwal 2021; Mahmoudi-Mehrizi and Ghanbari 2021), using the helical piles under the tunnel can be effective for mitigating the tunnel uplift. However, there is a lack of information on the uplift resistance of the helical piles in liquefied soils during an earthquake. In the present study, the performance of tunnels with helical piles against the tunnel uplift was investigated. The tests were carried out with 1*g* shaking table tests with sinusoidal excitation. The effects of pile length, number of the pile helix, and the distances between piles were compared through different model tests. The EPWP around the tunnels was investigated, and the uplift mechanism was focused. Also, the safety factor against uplift was calculated for each tunnel.

## Mechanism of the Helical Pile and Tunnel Uplift in Liquefied Sand

The interaction between the tunnel, the helical piles, and the surrounding soil should be described for the theoretical study of embedded helical piles and buried structures in liquefiable sand. Fig. 1 depicts the simplified mechanism of forces that induced uplift and resisting forces on soil wedge during liquefaction. Several researchers studied the sand dilatancy effect on the uplift resistance of pipelines and plates in the sand (Liu et al. 2012; Bolton 1987; White et al. 2008; Giampa et al. 2017). The truncated cone failure mechanism was considered as an acceptable method for predicting the uplift capacity of embedded helical piles. White et al. (2008) assumed that the inclination angle ($\psi$) was equal to the sand dilation angle.

For tunnels, the resisting forces are the soil shear strength ($F_{ST}$), the overlying soil weight ($F_{WT}$), and the structure weight ($F_T$). On the other hand, the buoyant force ($F_B$) is the active force for tunnels in the static condition. The forces related to the tunnel in the static condition can be calculated through Eqs. (1)–(3). In a dynamic condition, the excess pore pressure force ($F_{EPP}$) contributes to the active forces, enhancing the uplift potential. Furthermore, when EPWP generation occurs, the effective stress of the soil reduces, resulting in a decrease in the friction forces acting on the slip surfaces. The reduction in soil shear strength ($F_{ST}$) is assumed to be proportional to the excess pore pressure ratio ($r_u$) and can be estimated using Eq. (4).

In the static condition:

$$F_{WT} = \gamma' \cdot D_T \cdot \left(H_T - \frac{\pi \cdot D_T}{8}\right) + \gamma' \cdot H_T^2 \cdot \tan\psi \tag{1}$$

$$F_{ST} = \gamma' \cdot H_T^2 \cdot (\tan\varphi - \tan\psi) \cdot \left[\frac{(1+k_0)}{2} - \frac{(1-k_0)}{2} \cdot \cos 2\psi\right] \tag{2}$$

$$F_B = \gamma_w \cdot \frac{\pi \cdot D_T^2}{4} \tag{3}$$

In the dynamic condition:

$$F_{ST} = (1-r_u) \cdot \left\{\gamma' \cdot H_T^2 \cdot (\tan\varphi - \tan\psi) \cdot \left[\frac{(1+k_0)}{2} - \frac{(1-k_0)}{2} \cdot \cos 2\psi\right]\right\} \tag{4}$$

$$F_{EPP} = U_{EPP} \cdot D_T \tag{5}$$

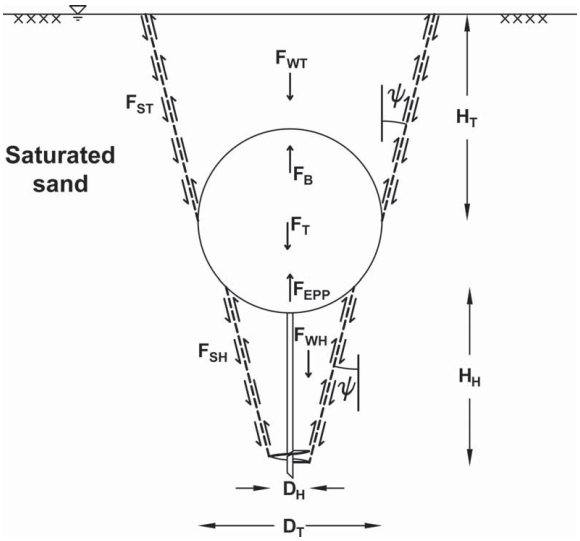


**Fig. 1.** Interaction between the tunnel and helical pile buried in saturated sand.

where $U_{EPP}$ = excess pore pressure at the bottom of the tunnel; $\gamma'$ = immersed unit weight of the saturated soil; $D_T$ = tunnel diameter; $H_T$ = tunnel buried depth up to the tunnel axis; $\psi$ = inclination angle; $\varphi$ = internal friction angle; and $k_0$ = lateral earth pressure. The ultimate uplift resistance of helical piles ($Q_u$) is the sum of shear resistance along the failure wedge surface ($F_{SH}$) and lifted soil block's weight ($F_{WH}$). The mobilized shear stress ($\tau_{SH}$) and shear resistance force along the slip surface with the existence of helical piles can be computed by Eqs. (7)–(9). Also, the lifted soil block weight overhead the helical pile was determined by Eq. (10).

$$Q_u = F_{WH} + F_{SH} \tag{6}$$

$$\tau_{SH} = \gamma' \cdot H_H \cdot (\tan\varphi - \tan\psi)\left[\frac{(1+K_0)}{2} - \frac{(1-K_0)\cdot\cos 2\psi}{2}\right] \tag{7}$$

$$A_f = 2\pi \int_0^{H_H} \left[\frac{D_H}{2} + (H_H - Z)\cdot\tan\psi\right] dZ \tag{8}$$

$$F_{SH} = (1-r_u)\left\{\gamma' \cdot H_H^2 \cdot (\tan\varphi - \tan\psi)\cdot\left(\frac{(1+K_0)}{2} - \frac{(1-K_0)\cdot\cos 2\psi}{2}\right)\right\} \tag{9}$$

$$F_{WH} = \gamma' \cdot H_H \cdot (D_H + H_H \cdot \tan\psi) \tag{10}$$

where $H_H$ = distance between the bottom helix and the bottom of tunnel. The resistive forces associated with the helical piles must assist the resistive forces of tunnels in overcoming the active forces during and after the earthquake to avoid the structure from being uplifted.

$$(F_{WT} + F_{ST} + F_T) + (F_{WH} + F_{SH}) > F_B + F_{EPP} \tag{11}$$

### Test Apparatus and Similitude Law

The uplift mitigation of circular tunnels with helical piles was studied using the shake table equipment at Semnan University. Fig. 2 shows the shaking table with sand rainer and other details of the system. The one-dimensional (1D) shaking table with the maximum payload of 20,000 N and 2 m × 3 m dimension were utilized for the tests. The device has a frequency range of 1–5 Hz along the length direction and a maximum displacement of 25 mm. The soil box with rigid walls and inner dimensions of 1,200 mm (length) × 900 mm (width) × 900 mm (height) was used for model preparation. The similitude law introduced by Iai (1989) for the 1 g shaking table tests was used in this study. Due to the limitation in soil box height (900 mm), the scale factor of the prototype to model was 32 ($N = 32$) for modeling 30 m soil depth. In another study, Haddad et al. (2022) used this shaking table to study the liquefaction phenomenon on the performance of suction caisson foundations. The results are presented in the model scale except otherwise stated. Table 1 presents the scaling factors for various geotechnical parameters in the shaking table tests.

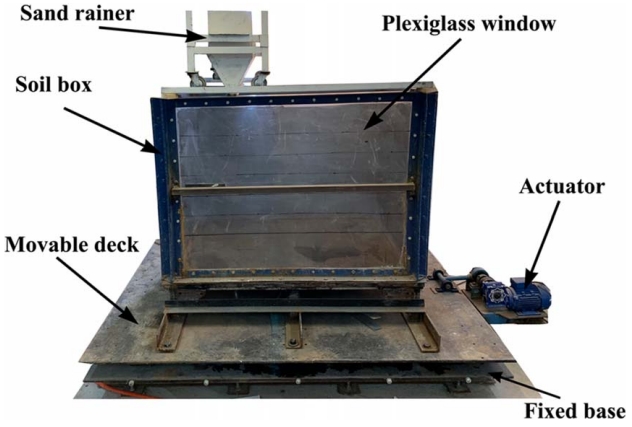


**Fig. 2.** 1 g shaking table with soil box, sand rainer, and other details.

### Tunnel and Helical Piles

The prototype tunnel model assumed 350 mm thick reinforced concrete, 4.8 m internal diameter, and 10 m buried depth in the liquefiable sand, which became a cylindrical asbestos model with 10 mm thickness and 150 mm inner diameter. The buried depth was twice ($2D_T$) the tunnel diameter (300 mm) from the ground surface up to the top of the tunnel. The properties of the tunnel model were fixed for all tests to consider similar conditions in this research. Both sides of the tunnel models were closed with transparent glass and sealed with glue. For applicable displacement of models inside the shaking box, a gap was considered between the two ends of the models and the sides of the shaking box.

In this study, three types of helical piles were manufactured to investigate the effect of helical piles as a mitigation method of the tunnels with uplift probability in liquefiable soil. Fig. 3 represents the schematic view of the pile models and the helical piles installed in the tunnels in this study. The pile length and the helix diameter were selected based on applicable in situ installation. Table 2 shows how the length of pile models ($L$), the number of helical piles along the tunnel ($N_P$), and the number of helixes on helical piles ($N_h$) were altered in each model. Other parameters of the models were constant in each test, like the shaft diameter ($S_d$) = 0.01 m, the helix diameter ($D_H$) = 0.03 m, the helix thickness ($t$) = 0.001 m, and the pitch ($P$) = 0.01 m.

Consequently, in previous studies, the distance between the helixes ($S_h$) has been classified based on whether the soil is sandy or clayey. Soil type and spacing between the helical plates are the main reason for the mobilization of the soil cylinder formed or individual helix mechanism between the upper and lower helixes (Sakr 2009). Most previous studies indicated that almost $3D_H$ distance between the helixes would individually mobilize the sandy soil between the helixes, and the cylindrical failure does not occur in the soil adjacent to the pile (Lutenegger 2011; El Sharnouby and El Naggar 2011). However, this value is recommended for nonliquefied soil. A spacing of $2D_H$ was chosen between the helixes to get the best performance of the uplift resistance. Hence, the maximum number of helixes can be used on the pile length, and almost an individual performance of sand mobilization is created.

### Soil Properties

The tests had been performed with Babolsar sand, which is a poorly graded sand and classified as SP according to the Unified Soil

**Table 1.** Scaling factors for different parameters used in the 1 g shaking table test

| Parameters | Prototype/model | Prototype/model ($N = 32$) |
|---|---|---|
| Density (kN/m$^3$) | 1 | 1 |
| Length (m) | N | 32 |
| Stress (kN/m$^2$) | N | 32 |
| Shear modulus (Pa) | N$^{0.5}$ | 5.66 |
| Acceleration (m/s$^2$) | 1 | 1 |
| Dynamic time (s) | N$^{0.75}$ | 13.45 |

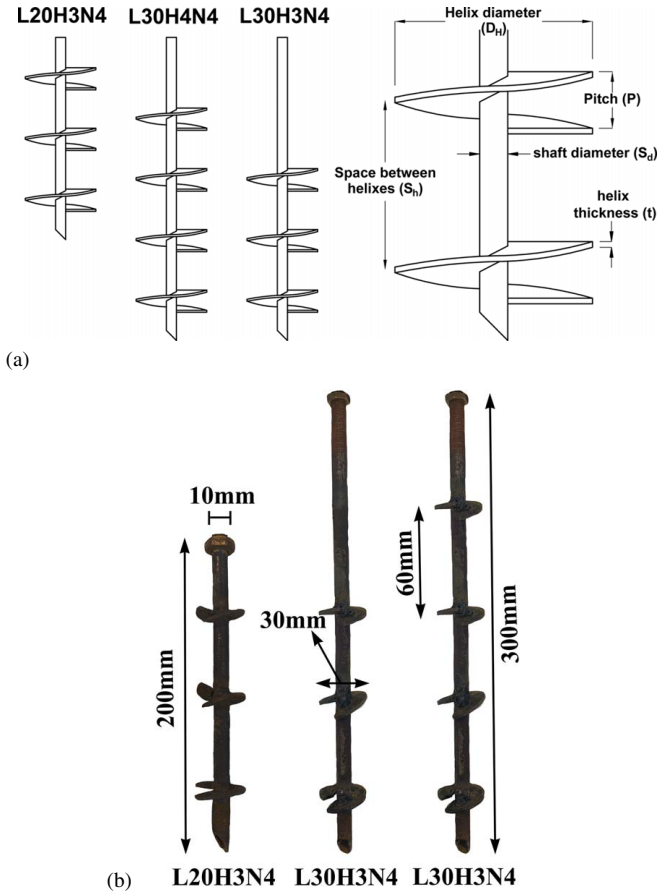


**Fig. 3.** Helical pile models: (a) schematic view of the helical piles; and (b) helical piles of the installed tunnels.

**Table 2.** Dimensions of tunnel models

| Model ID | Length of pile models ($L$) | Number of helical piles along the tunnel ($N_P$) | Number of helixes on helical piles ($N_h$) |
|---|---|---|---|
| L20H3N4 | 0.2 m | 4 | 3 |
| L30H4N4 | 0.3 m | 4 | 4 |
| L30H4N5 | 0.3 m | 5 | 4 |
| L30H3N4 | 0.3 m | 4 | 3 |

Note: The model IDs are selected according to the length of piles, helix diameter, and the number of helical piles along the tunnel length.

Classification System. The soil properties are presented in Table 3. Jafarian et al. (2013, 2020, 2021) enounced that Babolsar sand has liquefaction potential. This silicate sand with mentioned physical characteristics exists in a wide area on the southern coast of the Caspian Sea in Mazandaran, Iran. The grain size distribution of Babolsar sand is shown in Fig. 4.

### Model Preparation and Testing Program

The sand deposit was produced inside the shaking box by precipitating method, with a relative density ($D_r$) of 30% ± 1%. In ordert to have the same relative density conditions in all the tests, the dropping of the sand particles into the water from a specific distance was controlled. The soil experimented with a mold to find the optimum sand raining height before the shaking table test to reach the target relative density. It was determined that pouring the dry sand from a height of 100 mm into the box with a water

**Table 3.** Sand properties

| Property | Value |
|---|---|
| Specific gravity, $G_s$ | 2.73 |
| Average grain size, $D_{50}$ (mm) | 0.24 |
| Critical state friction angle, $\varphi$ (°) | 36 |
| Maximum void ratio, $e_{max}$ | 0.8 |
| Minimum void ratio, $e_{min}$ | 0.57 |
| Relative density, $D_r$ (%) | 30 |

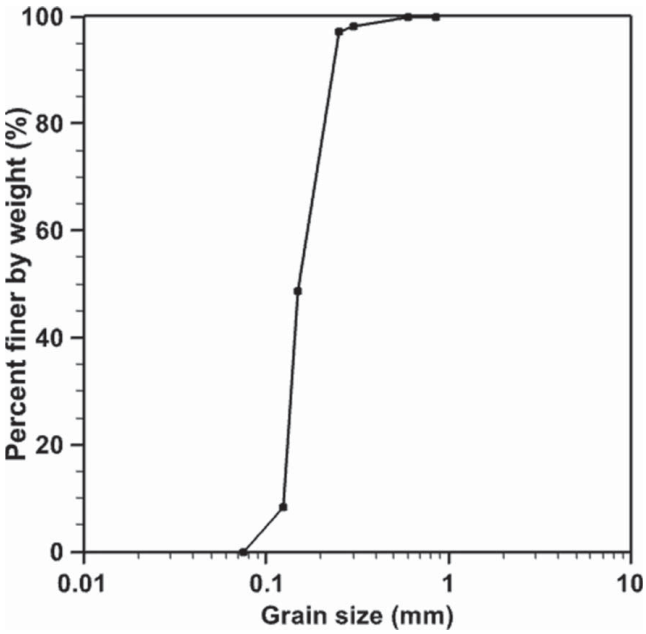


**Fig. 4.** Grain size distribution of sand.

level of 200 mm creates the desired loose relative density. The whole soil deposit was designed to be 800 mm depth, with a 650 mm loose sand layer overlying 150-mm-dense sand. After precipitating 150 mm of the soil layer, an excitation with 0.25 g amplitude was applied three times to attain the considered dense layer. After that, the loose layer was deposited inside the soil box.

The installation of helical piles in the soil was done simultaneously with the deposition of the loose layer. The helical piles were installed when the surface of the sand layer reached the intended depth for connecting the helical piles to the tunnel model. The piles were penetrated into the soil by a guide rod and installed perpendicularly to the soil surface. The penetration speed was 20 s per revolution to minimize soil disturbance. According to Wang et al. (2020), the rotation speed of the helical piles during installation will affect the soil condition and the uplift results. Therefore, the piles were installed at the same speed of rotation in all tests.

Two-piece belts were used to connect the helical piles in the tunnel model. The lower half of the belts were attached to the top of the piles after installing the helical piles in the soil (Fig. 5). Then, the tunnel was fixed in place on the lower half of the belt. After that, the upper half was fixed on the tunnel. Finally, the soil layer was completed to the designed elevation. The belts have a low thickness and weight and are rigidly fastened around the tunnel. This type of connection assures a negligible impact of the connection on the seismic performance of the piles, tunnel, and surrounding soil. Only the connection part of the two detachable pieces of the belts may reduce the uplift, which was ignored according to the similar circumstances formed in all models.

**Fig. 5.** Lower half of the belts, after screwing to the helical piles to connect to the tunnel.

The sensors were positioned at the specified locations when the soil was simultaneously precipitated in the test box. Excess pore pressure transducers (PPT), accelerometers (ACC), and linear variable differential transformer (LVDT) sensors were installed in the models. The excess PPT and the ACC sensors were placed on three levels; the top, side, and bottom around the structure. The LVDT was fixed over the container to measure the tunnel uplift. A steel alloy rod was installed on top of the tunnel model with a plate to locate the LVDT. The LVDT measured the vertical displacements of the tunnel, which presented an accurate measurement of the free uplift of the tunnel. Huang et al. (2015) used the same method to investigate the pipeline buried in medium-density sand. Fig. 6 shows the details of piles, tunnels, sensors, connection belts, and their locations for each test.

### Input Motion

Each test model was examined using two horizontal harmonic sinusoidal waves. Fig. 7 shows the sinusoidal time history of base motions with amplitudes of 0.14 and 0.17 g. Both excitations had 9 s duration but different frequencies (0.14 g had a frequency of 3.5 Hz and 0.17 g of 4 Hz). The applied accelerations were chosen based on the specifications and performance of the shaking table system. Furthermore, due to the required thickness of liquefaction extent in the sand deposit, it was necessary to apply acceleration with the amplitudes used in the experiments that produced frequencies of 3.5 and 4 Hz according to the available shaking table. Shaking of 0.14 and 0.17 g would be called EX1 and EX2, respectively.

## Tests Results and Discussion

### Free Field Test

An understanding of the soil conditions is required during liquefaction for comprehending the behavior of structures in liquefiable soil. Hence, a free field test without any tunnel model was carried out besides the main tests of the research to assess the depth of the liquefied layer. Also, the soil conditions surrounding the tunnel and helixes of each pile can be compared with the soil in the free field. The test was performed with two accelerations in a row (EX1 and EX2). The excitations were applied at time intervals to the soil deposit for the EPWP dissipation and reconsolidation process. According to the described conditions at the beginning of the experiment, the relative soil density was 30% and reached 45% after applying EX1 acceleration. The density was determined using the final soil settlement after EX1. The EPWP history validated the soil liquefaction capability of sand during the second excitation.

The EPWP generation was evaluated in the free field test by putting the PPT at different depths. The EPWP is shown in Fig. 8. According to the line $r_u = 1$, the depth of the complete liquefied layer at EX1 acceleration has reached 0.45 m. The depth of the liquefied layer has increased with the acceleration of EX2 and reached 0.55 m depth from the soil surface in a complete liquefied condition. In this manner, it was possible to establish the position of each helical pile than the liquefied sand. EPWP changes at the different soil depths indicate the liquefaction conditions observed in both excitations. In the centrifuge tests, Mehrzad et al. (2016, 2018) and Jafarian et al. (2017) reported faster EPWP generation and dissipation with delay in the shallow sand deposit and an increase in the liquefaction extent by more severe acceleration. These results confirm the liquefaction conditions in the current study.

### Effect of Helical Pile Length on Uplift Displacement

The use of helical piles require precise design against uplifting. The efficiency of the helical pile against uplift would dramatically decrease in low shear strength soft soil during liquefaction. Hence, one of the important characteristics of helical piles is pile length, which requires special consideration during liquefaction. In this study, piles with lengths of 200 mm (L20H3N4) and 300 mm (L30H3N4) were chosen based on the findings of the free field test. Other characteristics of the helical piles were the same, such as the number of helical piles along with the model and the number and diameter of helixes.

Besides the uplift time history of L20H3N4 and L30H3N4, Fig. 9 depicts the $r_u$ condition according to the EPWP results of the free field test. With EX1 excitation, all three helixes of L20H3N4 were placed in liquefied soil with $r_u < 1$. Although $r_u < 1$, the EPWP was still high based on Fig. 8, and the soil condition was close to complete liquefaction. While applying EX2, one helix was completely immersed in fully liquefied soil, and the other two helixes were placed in the sand with $r_u < 1$. By extending the pile length and helix penetration at the lower depths, two helixes of the L30H3N4 pile were positioned in dense soil, creating a more stable condition for the structure and piles system. Because of these differences, Fig. 9 shows the uplift time history of the models used compared with the model without helical piles (D15H30). Table 4 also shows the displacement of the models during the shaking, after the shaking, and during the settling.

Comparisons revealed that during EX1 shaking, the L30H3N4 uplifting velocity was slower than the other two models for most of the shaking duration due to the soil condition around the piles seen in Fig. 9. However, with EX2, the uplift velocity of L30H3N4 also became close to the L20H3N4 and D15H30. Of course, in the postshaking period, the L20H3N4 did not have significant performance, but the L30H3N4 model mitigated the uplift. The presence of helixes even increased the settlement during the settlement period. However, the utilization of helical piles for tunnels had been effective during the liquefaction, and it is clear that the overall uplift had decreased.

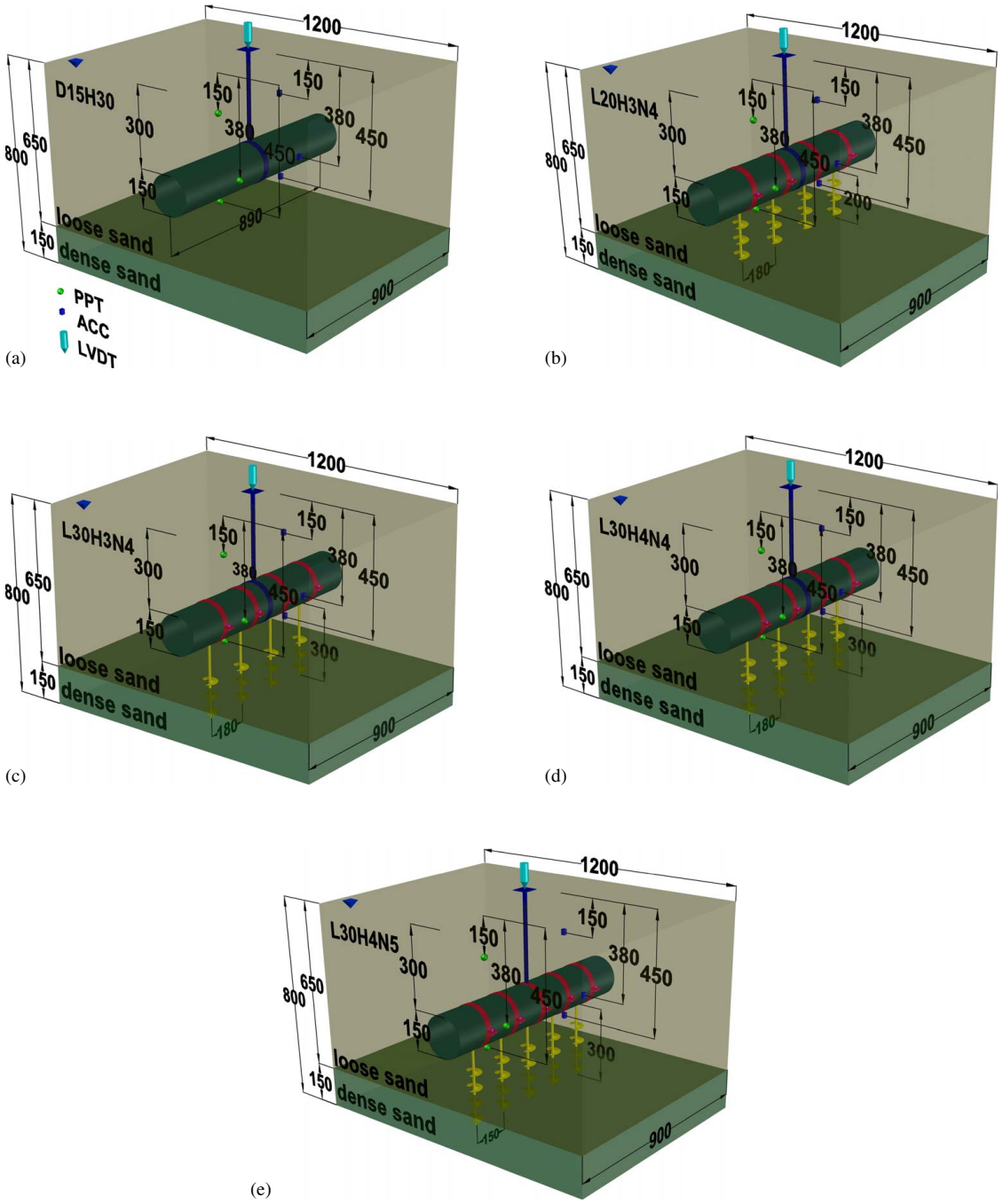


**Fig. 6.** 3D view of the model tests layout conducted in the shaking table test: (a) D15H30 (tunnel without helical piles); (b) L20H3N4 (pile length = 200 mm, helix number = 3, pile number = 4); (c) L30H3N4 (pile length = 300 mm, helix number = 3, pile number = 4); (d) L30H4N4 (pile length = 300 mm, helix number = 4, pile number = 4); and (e) L30H4N5 (pile length = 300 mm, helix number = 4, pile number = 5) (dimensions are in mm).

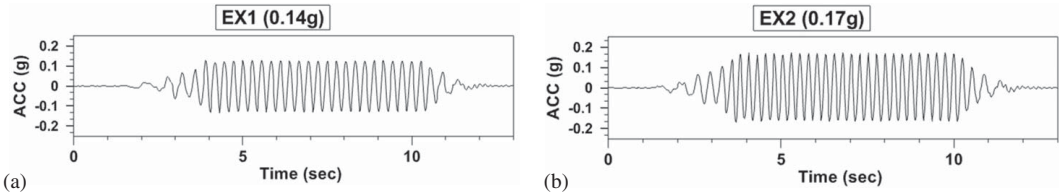


**Fig. 7.** Base input motions: (a) EX1; and (b) EX2.

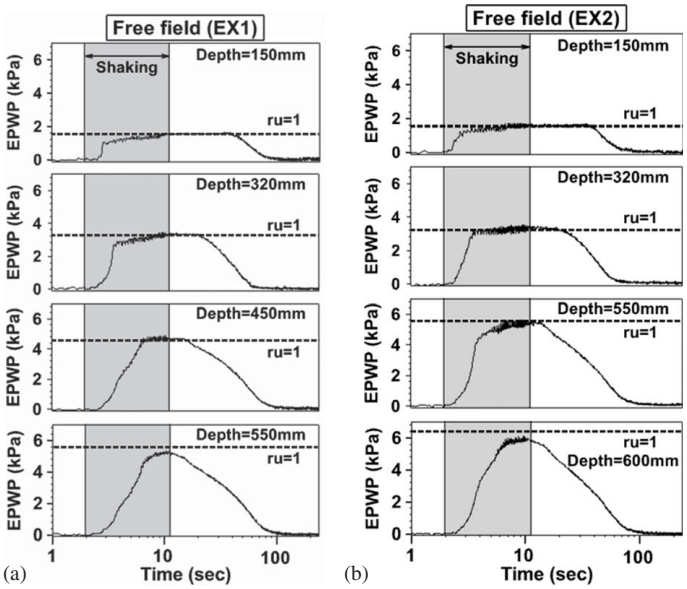


**Fig. 8.** EPWP time histories recorded at free field test: (a) EX1; and (b) EX2.

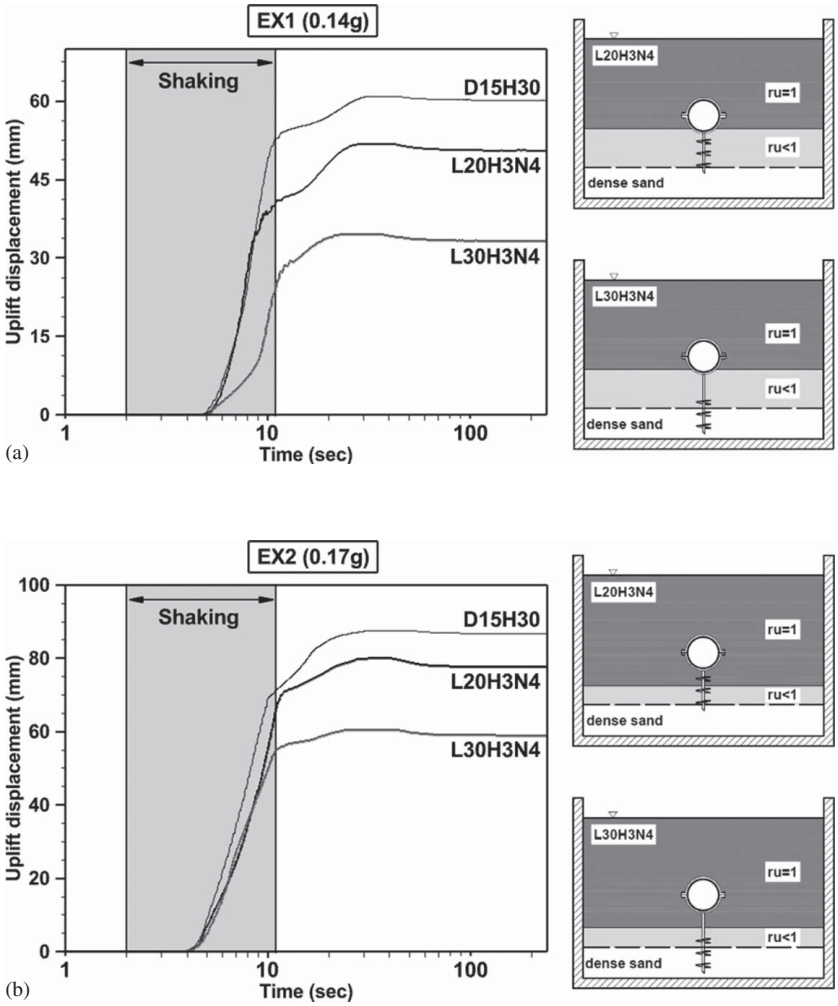


**Fig. 9.** Effect of helical piles with different lengths on the uplift of the tunnel in comparison with the tunnel without helical piles: (a) EX1; and (b) EX2.

There are three reasons for reducing the uplift by increasing the pile length. Placing the helical piles on soil with lower porosity and greater shear strength can enable the helixes to be more successful in minimizing liquefaction-induced uplift. A deeper helical pile increases the soil weight above the helixes and improves the uplift-resistant shear strength surface to resist uplift forces. Accordingly, the uplift can be minimized as much as possible by increasing the length of the helical piles.

### Effect of Helix Number on Uplift Displacement

For utilizing helical piles, it should be highlighted that there is an operational limit to the depth of penetration of these piles. As a result, four helixes were employed on the 300 mm length of L30H4N4 for efficient helical pile usage. L30H4N4 was compared with the helical pile with three helixes used at the bottom (L30H3N4). In general, these two models have the same characteristics, except the presence of the extra top helix creates a difference in the behavior of the models.

EX1 put the top helix of the L30H4N4 in soil with the $r_u < 1$ condition. As seen in Fig. 10, the uplift velocity had dropped more than L30H3N4, resulting in less uplift displacement during the shaking. Also, the postshaking uplift had decreased and diminished the overall uplift (Table 5). By applying EX2, the top helix of the L30H4N4 was placed in the complete liquefied zone. Consequently, the uplift velocity of both models was close but still L30H4N4 affected reducing the overall uplift. The settlement at the end of the test was also lowered by utilizing L30H4N4 at both applied accelerations.

**Table 4.** Uplift time history of D15H30, L20H3N4, and L30H3N4 during and after shaking and the settlement at the end of the tests

| Excitation | Test ID | Uplift during shaking (mm) | Uplift after shaking (mm) | Settlement (mm) |
|---|---|---|---|---|
| EX1 | D15H30 | 52.87 | 7.92 | 0.61 |
| | L20H3N4 | 40.55 | 11.29 | 1.27 |
| | L30H3N4 | 24.15 | 10.39 | 1.26 |
| EX2 | D15H30 | 71.25 | 16.27 | 0.81 |
| | L20H3N4 | 66.24 | 13.84 | 2.44 |
| | L30H3N4 | 54.76 | 5.78 | 1.59 |

### Effect of the Number of Helical Piles on Uplift Displacement

More helical piles along the underground track would be beneficial in decreasing the uplift. However, engineers are constantly attempting for the optimum design. As a result, in this experiment, helical piles at two different intervals from each other were examined. Beneath the structure, L30H4N4 was installed at $1.2D_T$ (diameter of

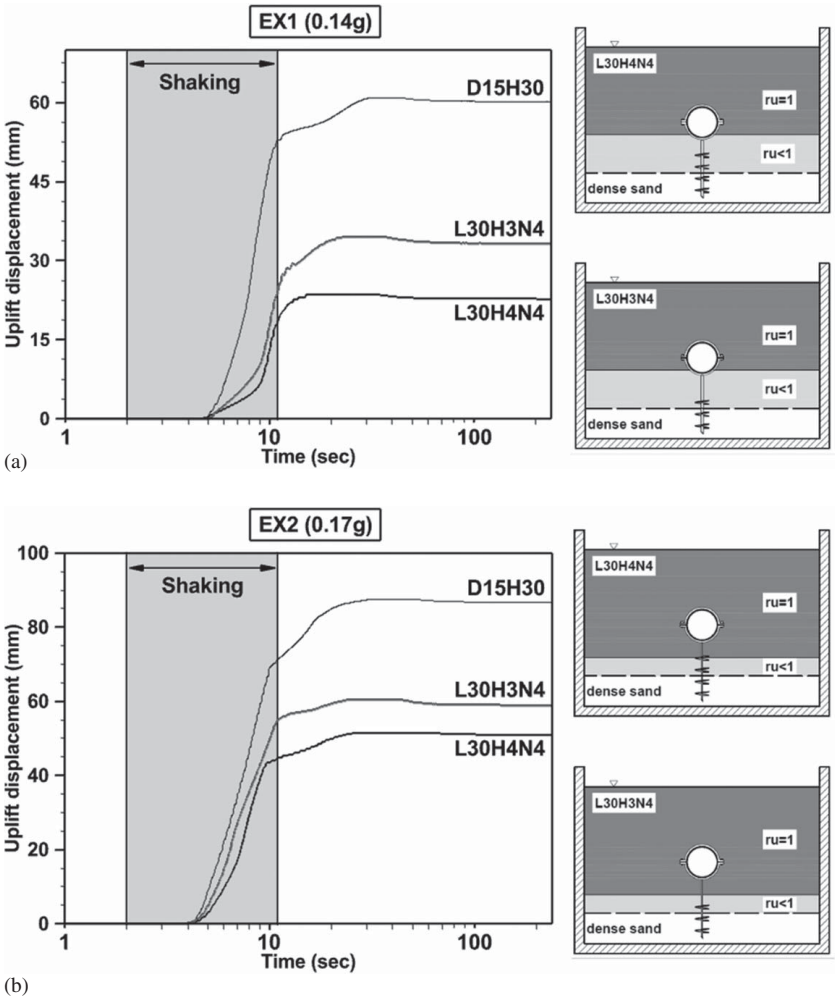


**Fig. 10.** Effect of helical piles with different helix numbers on the uplift of the tunnel in comparison with the tunnel without helical piles: (a) EX1; and (b) EX2.

**Table 5.** Uplift time history of D15H30, L30H3N4, and L30H4N4 during and after shaking and the settlement at the end of the tests

| Excitation | Test ID | Uplift during shaking (mm) | Uplift after shaking (mm) | Settlement (mm) |
|---|---|---|---|---|
| EX1 | D15H30 | 52.87 | 7.92 | 0.61 |
| | L30H3N4 | 24.15 | 10.39 | 1.26 |
| | L30H4N4 | 18.48 | 5.13 | 0.83 |
| EX2 | D15H30 | 71.25 | 16.27 | 0.81 |
| | L30H3N4 | 54.76 | 5.78 | 1.59 |
| | L30H4N4 | 44.69 | 6.85 | 0.52 |

**Table 6.** Uplift time history of D15H30, L30H4N4, and L30H4N5 during and after shaking and the settlement at the end of the tests

| Excitation | Test ID | Uplift during shaking (mm) | Uplift after shaking (mm) | Settlement (mm) |
|---|---|---|---|---|
| EX1 | D15H30 | 52.87 | 7.92 | 0.61 |
| | L30H4N4 | 18.48 | 5.13 | 0.83 |
| | L30H4N5 | 16.34 | 3.79 | 0.88 |
| EX2 | D15H30 | 71.25 | 16.27 | 0.81 |
| | L30H4N4 | 44.69 | 6.85 | 0.52 |
| | L30H4N5 | 35.17 | 10.52 | 2.39 |

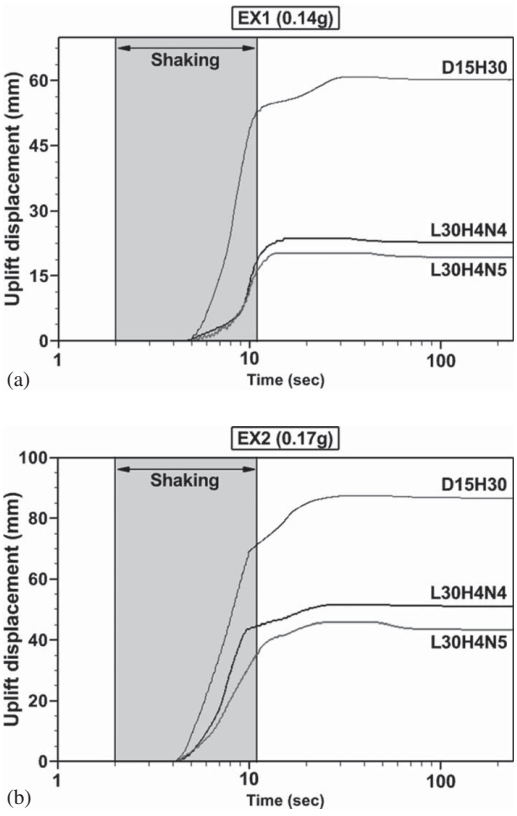


**Fig. 11.** Effect of helical piles with different pile intervals on the uplift of the tunnel in comparison with the tunnel without helical piles: (a) EX1; and (b) EX2.

the tunnel) distances, whereas L30H4N5 was located at $1D_T$ spacing. Other than the spacing between the piles, the model's characteristics were similar.

The uplift time history of both models revealed that the uplift velocity at EX1 was similar (Fig. 11). During EX1, L30H4N5 outperformed L30H4N4 by 4% in uplift. Furthermore, there was no dramatic decrease in postshaking rise, and the difference in overall uplift was limited. At EX2 acceleration, L30H4N5 had a lower uplift velocity than L30H4N4, and there was a 13% difference in model uplift at the end of the shaking. In addition, the models' settlement at the end of the test was similar in EX1 acceleration and increased in EX2 acceleration (Table 6).

According to the presented mechanism for helical piles, it was stated that the shear strength of the sand above each helical pile is effective in preventing the uplift. The overall performance of the helical piles on uplift mitigation would decrease with the proximity of the piles and restriction of the overlying soil shear strength mobilization for each pile (Fig. 12). As a result, selecting the number of helical piles is critical. Installing extra helical piles would cause efficiency loss because of the interference of shear surfaces at the soil on top of the helical piles. The pile intervals must be chosen based on the diameter of the helixes, the pile penetration depth, and the soil dilatancy angle to reduce interference in the shear strength performance of the soil above each pile.

### Excess Pore-Water Pressure around the Models

Investigating the EPWP around the tunnel can help to understand the uplift behavior of the structure during liquefaction. L30H4N4's uplift time history was shown to be similar to that of L30H4N5. Likewise, the uplift behavior of L30H3N4 was similar to that of L20H3N4. The same trend was repeated in the time history of EPWP. For this purpose, EPWP for L30H4N5 and L30H3N4 is shown in Fig. 13. Furthermore, the EX1 acceleration was evaluated based on the convergence of EPWP behavior at both accelerations.

Despite the presence of L30H4N5, the time history of EPWP at the top of the structure was similar to the free field, and the tunnel's impact was essentially small, as shown in Fig. 13. However, L30H3N4 generated higher EPWP at the beginning of the shaking, which led to soil softening and loss of shear strength. For this reason, L30H4N5 did not have tensile cracks, while L30H3N4 experienced it on the soil surface. The tensile crack occurrence caused a dramatic fall in EPWP and suction in the soil. The occurrence of tensile cracks was the cause of the large uplifting of L30H3N4 after the shaking. The tensile crack on the soil surface of L30H3N4 after the test is shown in Fig. 14. In addition, with the upward displacement of L30H3N4, rapid water dissipation was obtained, and EPWP was lower than L30H4N5.

### Acceleration Time History around the Models

The soil seismic behavior surrounding L30H3N4, L30H4N5, and D15H30 was analyzed, as was in the EPWP study because the models have similar acceleration time histories. The accelerations in the soil at the top, side, and bottom of the tunnels were measured and compared with that of free field conditions are shown in Fig. 15. The acceleration above the L30H4N5 was more similar to the free field, which makes sense given that no tension cracks occurred in this model and no drastic drop in EPWP has occurred. On the other hand, L30H3N4 and D15H30 (the model without helical pile) have a similar acceleration response at the top of the tunnel. This phenomenon is consistent with the tensile crack observation at the top of the tunnel and a dramatic drop in EPWP. However, the soil acceleration at the tunnel's sides and bottom showed almost the same response for all models. In general, the existence of tunnels, with or without helical piles, had a negligible impact on the seismic response of the soil at the tunnel's side and bottom. Moreover, the presence of the tunnel and the helical pile's installation

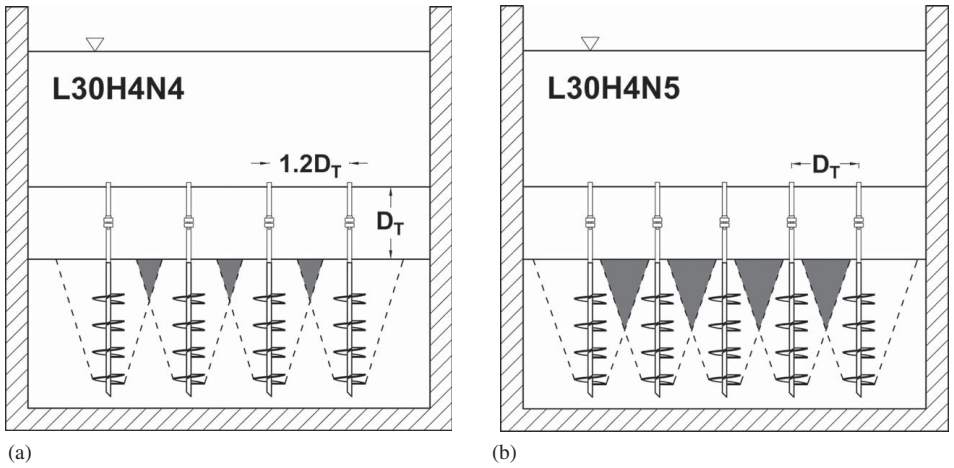


**Fig. 12.** Side view of the test box and the extent of interference of the overlying soil shear strength mobilization for (a) L30H4N4; and (b) L30H4N5.

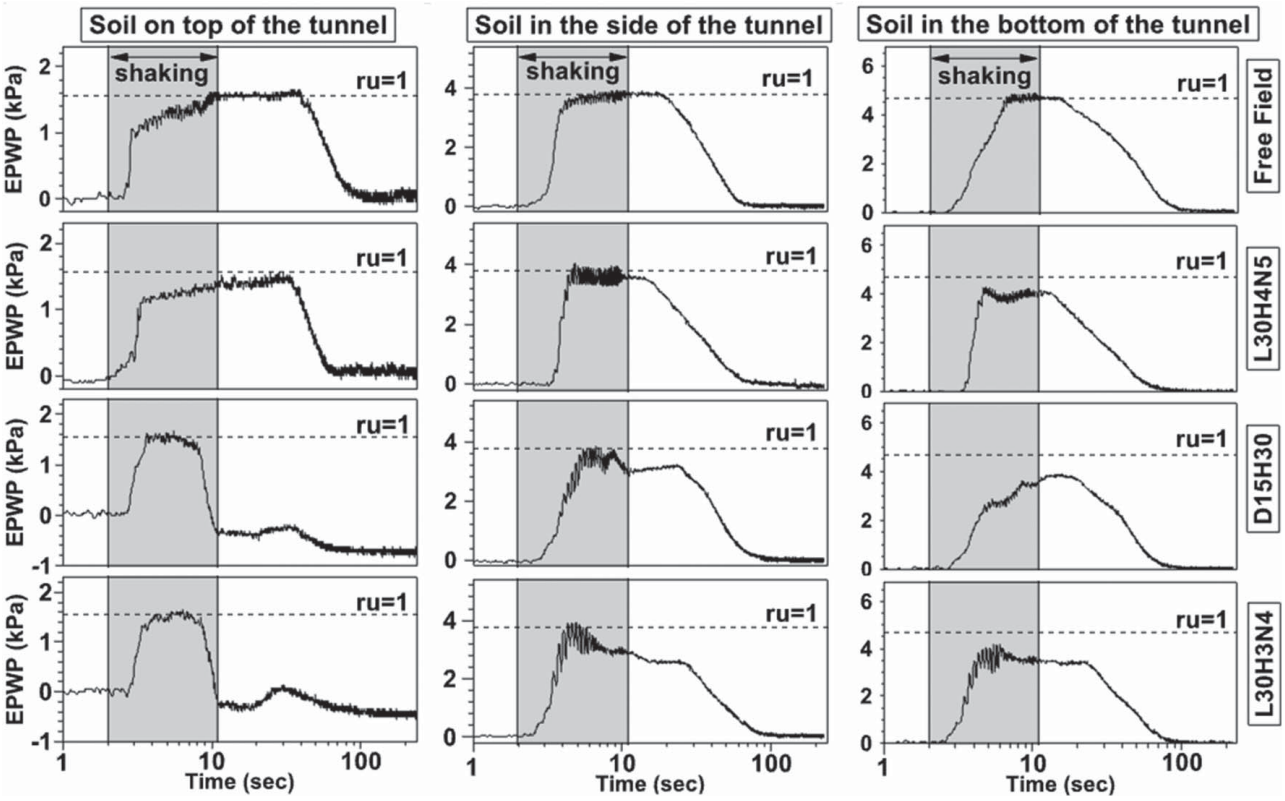


**Fig. 13.** EPWP at the free field (FF) and around L30H4N5, D15H30, and L30H3N4 with EX1(0.14 g) in each row.

had a considerable influence on the seismic performance of the liquefied soil on top of the tunnel.

### *Safety Factor of Tunnel with Helical Piles*

Calculating the safety factor (*FS*) of the tunnel during liquefaction can help to evaluate the uplift probability of the structure. Without utilizing any enhancement procedures, the safety factor of tunnels may be estimated using Eq. (12). Due to the utilization of helical piles in this investigation, extra forces were involved in determining the safety factor. According to the forces related to the helical piles, the safety factor in the presence of the helical piles was determined based on Eq. (13).

$$FS = \frac{F_{WT} + F_T + F_{ST}}{F_B + F_{EPP}} \tag{12}$$

$$FS = \frac{F_{WT} + F_T + F_{ST} + F_{SH} + F_{WH}}{F_B + F_{EPP}} \tag{13}$$

The forces associated with the tunnel and helical piles are calculated using Eqs. (1)–(5) and Eqs. (6)–(10), respectively. Fig. 16 compares the safety factor for the L30H4N5, as the most effective model, with the D15H30. Although the installation of helical piles enhanced the safety factor throughout the liquefaction time, it also

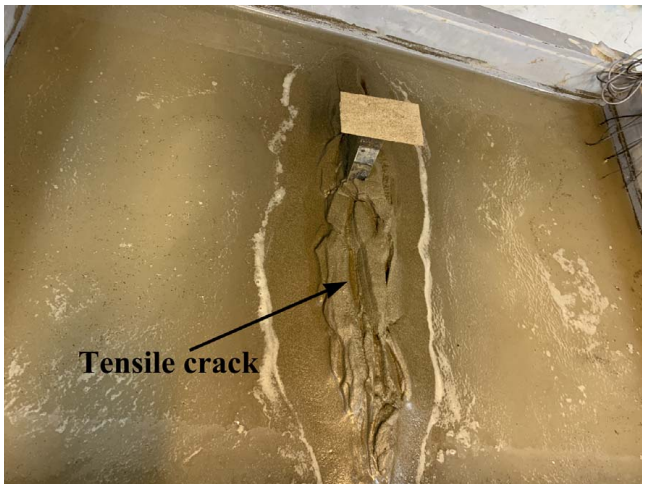


**Fig. 14.** Tensile crack at the soil surface of L30H3N4 after the test.

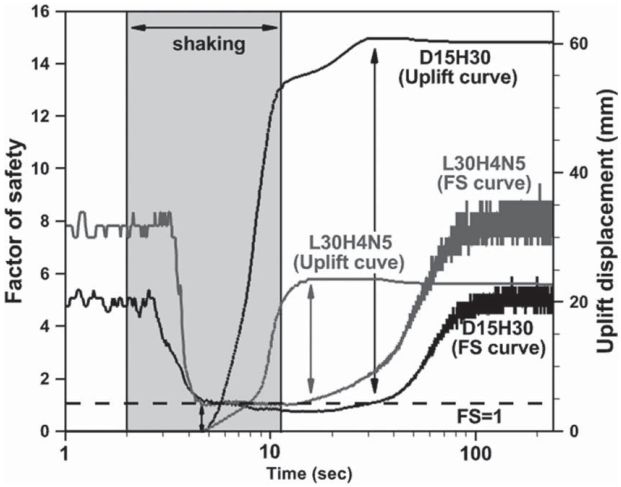


**Fig. 16.** Comparison between FS and tunnel uplift with EX1 (0.14 g).

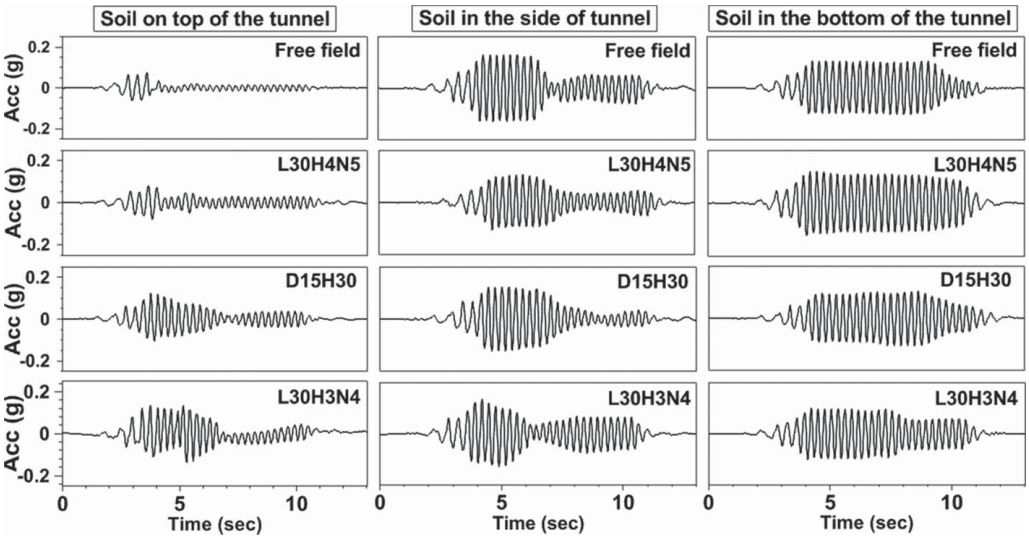


**Fig. 15.** Acceleration time history at the free field (FF) and around L30H4N5, D15H30, and L30H3N4 with EX1(0.14 g) in each row.

increased the safety factor under the static circumstances at the start of the test, which would be helpful in the submerged tunnels and onshore pipeline projects. Theoretically, triggering of the $FS = 1$ conditions indicates the starting point of the upward displacement, and the uplift would be ceased with getting out of the $FS = 1$ condition. According to Fig. 16, both models started uplifting with $FS = 1$ and terminated the upward displacement when $FS > 1$ happened. D15H30 had even experienced $FS < 1$ in the postshaking period, which caused significant upward displacement. However, L30H4N5 (with helical piles) quickly emerged from the unstable $FS = 1$ condition and had a limited amount of uplift after shaking time. In general, the uplift potential, the beginning point, and the time ceasing upward displacement may be calculated with sufficient certainty using the relationship of the safety factor derived using the equilibrium forces.

### *Uplift Mechanism and the Relationship between Uplift and EPWP*

It is required to investigate the uplift mechanism of the models to examine the performance of helical piles more precisely. Fig. 17 shows the relationship between EPWP at the overlying soil and model uplift in L30H4N5 and D15H30. The simplified uplift mechanism is also used to compare the two models (Fig. 18). The duration of data recording was separated into distinct phases to correctly assess the conditions of the models at each step of the experiment to evaluate the uplift mechanism.

EPWP was initially generated in both models with the onset of shaking until the complete liquefaction condition was reached. However, the D15H30 reached this point in a shorter time. According to the schematic perspective in Fig. 18, this has resulted in a rapid D15H30 uplift transition phase and primary phase with a steep slope. L30H4N5 reached complete liquefaction condition in the final few cycles of shaking and experienced a long-term uplift transfer phase that accounts for a significant portion of the shaking duration. It missed out on the possibility of achieving a substantial uplift with a steep slope in the primary uplift phase. The uplift time histories of the models without helical piles showed a short-term uplift transition phase followed by a long-term primary uplift phase, but the model with helical piles operated in reverse. The impact of helical piles on the primary uplift velocity of the models was insignificant, and L30H4N5 had a similar uplift velocity to

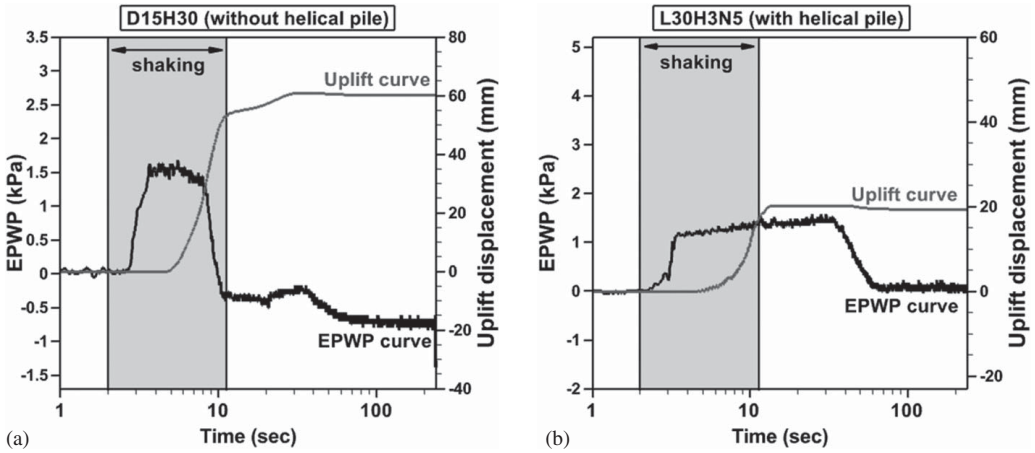


**Fig. 17.** Relation between EPWP at the overlying soil and uplift displacement mechanism with EX1(0.14 g): (a) without helical pile; and (b) with helical piles.

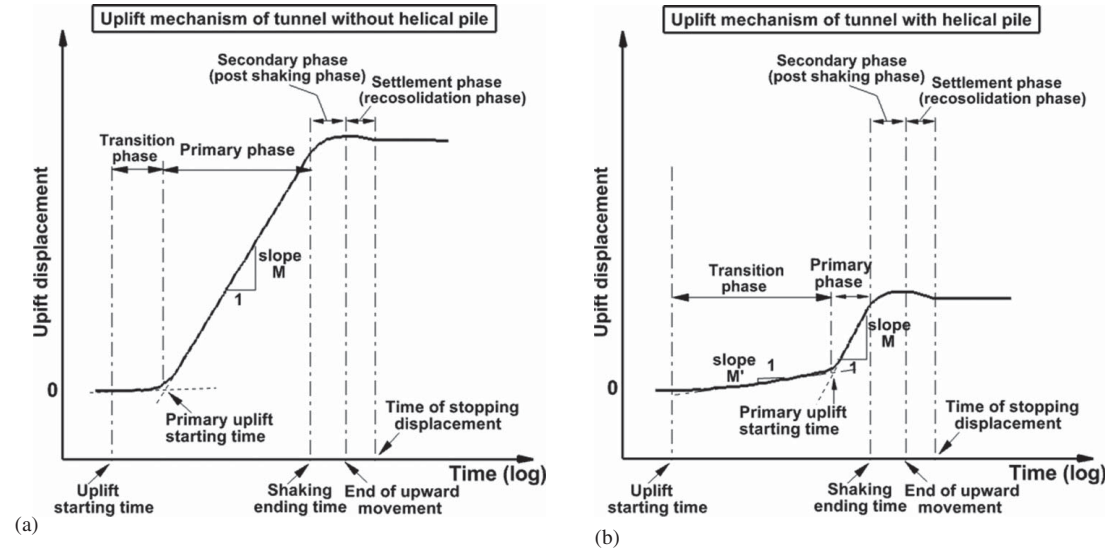


**Fig. 18.** Illustration of transition, primary phase, secondary phase, and settle down phase of shallow tunnel uplifting: (a) without helical piles; and (b) with helical piles.

D15H30. Another distinction between the two models was the presence of tensile cracks in the soil above D15H30, which results in higher uplift in the postshaking period than the model without helical piles. The postshaking settlement did not vary considerably, and the installation of helical piles had limited influence on the reconsolidation phase.

## Conclusion

In this study, helical piles are employed to decrease uplift of the tunnels placed in liquefied soil. The influence of pile length, helix number, and pile number is examined. Uplift mechanisms and EPWP in the surrounding soil are also evaluated for structures with and without helical piles. Tests are conducted in 1 g shaking table with a rigid box, and two sinusoidal accelerations with 0.14 and 0.17 g amplitudes are applied to the models. Results are explained based on the aforementioned situation. The results are as follows:

- Increasing the length of the piles, the number of helixes, and the number of helical piles reduces the uplift velocity and consequently mitigated upward displacement of the tunnels. Long helical piles have the chance of installing on dense sand with higher shear strength and more soil weight above the helixes and have improved resistant shear strength surface. However, it should be noted that in the optimal design of the helical pile characteristics, the maximum possible performance can be obtained.
- EPWP performs similarly to the free field in the soil covering the structure, and no tensile cracking occurs at the soil surface by utilizing tunnels with suitable performance helical piles (L30H4N4 and L30H4N5). However, the tunnels with severe uplift (D15H30, L20H3N4, and L30H3N4) that experienced tensile cracks encounter a significant decrease in EPWP, even though suction occurs in the soil above the tunnels.
- Tensile cracks also affect the acceleration time history of soil above the tunnels and amplify the acceleration amplitude; however, without tensile cracks, the acceleration in the soil above the tunnels is like the free field. Acceleration in the sand at the side and bottom of the tunnels is almost the same.
- Factor of safety is evaluated based on the equilibrium forces, and the result shows an acceptable estimation of the starting and ceasing the uplift. Furthermore, it reveals that the helical piles could help to increase the factor of safety against uplift.

- The uplift mechanism of models with helical piles is investigated, and it is discovered that the main effect of helical piles was relevant to the uplift transition phase. As a result, while the duration of the uplift transition phase increases, most of the shaking period passes, and the primary phase is limited to a few last shaking cycles. Also, postshaking uplift occurs to a limited extent due to the elimination of tensile cracking.

## Data Availability Statement

All data, models, or codes that support the findings of this study are available from the corresponding author upon reasonable request.

## Acknowledgment

The authors acknowledge the Department of Civil Engineering, Semnan University, for providing equipment.

## References

Adalier, K., T. Abdoun, R. Dobry, R. Phillips, D. Yang, and E. Naesgaard. 2003. "Centrifuge modelling for seismic retrofit design of an immersed tube tunnel." *Int. J. Phys. Modell. Geotech.* 3 (2): 23–35. https://doi.org/10.1680/ijpmg.2003.030203.

Bao, X., Z. Xia, G. Ye, Y. Fu, and D. Su. 2017. "Numerical analysis on the seismic behavior of a large metro subway tunnel in liquefiable ground." *Tunnelling Underground Space Technol.* 66: 91–106. https://doi.org/10.1016/j.tust.2017.04.005.

Bolton, M. D. 1987. "Discussion: The strength and dilatancy of sands." *Geotechnique* 37 (2): 219–226. https://doi.org/10.1680/geot.1987.37.2.219.

Castiglia, M., F. S. de Magistris, S. Morgante, and J. Koseki. 2019. "Geogrids as a remedial measure for seismicliquefaction induced uplift of onshore buried gas pipelines." In *National Conf. of the Researchers of Geotechnical Engineering*, edited by F. Calvetti, F. Cotecchia, A. Galli, and C. Jommi, 649–657. Cham, Switzerland: Springer.

Castiglia, M., F. S. de Magistris, and A. Napolitano. 2018. "Stability of onshore pipelines in liquefied soils: Overview of computational methods." *Geomech. Eng.* 14 (4): 355–366. https://doi.org/http://doi.org/10.12989/gae.2018.14.4.355.

Castiglia, M., S. Morgante, A. Napolitano, and F. S. de Magistris. 2017. "Mitigation measures for the stability of pipelines in liquefiable soils." *J. Pipeline Eng.* 16 (3): 115–139.

Chen, W. W., B. J. Shih, C. W. Wu, and Y. C. Chen. 2000. "Natural gas pipeline system damages in the Ji-Ji earthquake (The City of Nantou)." In *Proc., 6th Int. Conf., on Seismic Zonation*. Oakland, CA: Earthquake Engineering Research Institute.

Chian, S. C., and S. P. G. Madabhushi. 2012. "Effect of buried depth and diameter on uplift of underground structures in liquefied soils." *Soil Dyn. Earthquake Eng.* 41: 181–190. https://doi.org/10.1016/j.soildyn.2012.05.020.

Chian, S. C., and K. Tokimatsu. 2012. "Floatation of underground structures during the $M_w$ 9.0 Tōhoku Earthquake of 11th March 2011." In *Proc., 15th World Conf. on Earthquake Engineering*. Lisbon, Portugal: Sociedade Portuguesa de Engenharia Sismica (SPES).

Chian, S. C., K. Tokimatsu, and S. P. G. Madabhushi. 2014. "Soil liquefaction-induced uplift of underground structures: Physical and numerical modeling." *J. Geotech. Geoenviron. Eng.* 140 (10): 04014057. https://doi.org/10.1061/(ASCE)GT.1943-5606.0001159.

Chou, J. C., B. L. Kutter, T. Travasarou, and J. M. Chacko. 2011. "Centrifuge modeling of seismically induced uplift for the BART transbay tube." *J. Geotech. Geoenviron. Eng.* 137 (8): 754–765. https://doi.org/10.1061/(ASCE)GT.1943-5606.0000489.

Das, B. M., and G. R. Seeley. 1975. "Breakout resistance of shallow horizontal anchors." *J. Geotech. Eng. Div.* 101 (9): 999–1003. https://doi.org/10.1061/AJGEB6.0000202.

Dickin, E. A. 1988. "Uplift behavior of horizontal anchor plates in sand." *J. Geotech. Eng.* 114 (11): 1300–1317. https://doi.org/10.1061/(ASCE)0733-9410(1988)114:11(1300).

El Sharnouby, M., and M. El Naggar. 2011. "Monotonic and cyclic axial full-scale testing of reinforced helical pulldown micropiles." In *Proc., of the 2011 Pan-American Conf. on Soil Mechanics and Geotechnical Engineering 64th Canadian Geotechnical Conf.* London: ISSMGE.

Giampa, J. R., A. S. Bradshaw, and J. A. Schneider. 2017. "Influence of dilation angle on drained shallow circular anchor uplift capacity." *Int. J. Geomech.* 17 (2): 04016056. https://doi.org/10.1061/(ASCE)GM.1943-5622.0000725.

Guner, S., and S. Chiluwal. 2021. "Cyclic load behavior of helical pile-to-pile cap connections subjected to uplift loads." *Eng. Struct.* 243: 112667. https://doi.org/10.1016/j.engstruct.2021.112667.

Haddad, A., A. Barari, and R. Amini. 2022. "The remedial performance of suction caisson foundations for offshore wind turbines under seismically induced liquefaction in the seabed: Shake table testing." *Mar. Struct.* 83: 103171. https://doi.org/10.1016/j.marstruc.2022.103171.

Huang, B., J. Liu, D. Ling, and Y. Zhou. 2015. "Application of particle image velocimetry (PIV) in the study of uplift mechanisms of pipe buried in medium dense sand." *J. Civ. Struct. Health Monit.* 5 (5): 599–614. https://doi.org/10.1007/s13349-015-0130-y.

Iai, S. 1989. "Similitude for shaking table tests on soil-structure-fluid model in 1g gravitational field." Soils Found. 29 (1): 105–118. https://doi.org/10.3208/sandf1972.29.105.

Ilamparuthi, K., E. A. Dickin, and K. Muthukrisnaiah. 2002. "Experimental investigation of the uplift behaviour of circular plate anchors embedded in sand." *Can. Geotech. J.* 39 (3): 648–664. https://doi.org/10.1139/t02-005.

Jafarian, Y., P. Esmaeilpour, S. Shojaeemehr, H. Taghavizade, S. Rouhi, and J. S. McCartney. 2021. "Impacts of fixed-end and flexible boundary conditions on seismic response of shallow foundations on saturated sand in 1-g shaking table tests." *Geotech. Test. J.* 44 (3): 637–664. https://doi.org/10.1520/GTJ20200018.

Jafarian, Y., A. Ghorbani, S. Salamatpoor, and S. Salamatpoor. 2013. "Monotonic triaxial experiments to evaluate steady-state and liquefaction susceptibility of Babolsar sand." *J. Zhejiang Univ. Sci.* 14: 739–750. https://doi.org/10.1631/jzus.A1300032.

Jafarian, Y., B. Mehrzad, C. J. Lee, and A. H. Haddad. 2017. "Centrifuge modeling of seismic foundation-soil-foundation interaction on liquefiable sand." *Soil Dyn. Earthquake Eng.* 97: 184–204. https://doi.org/10.1016/j.soildyn.2017.03.019.

Jafarian, Y., H. Taghavizade, S. Rouhi, S. Shojaemehr, and P. Esmaeilpour. 2020. "Shaking table experiments to evaluate the boundary effects on seismic response of saturated and dry sands in level ground condition." *Int. J. Civ. Eng.* 18 (7): 783–795. https://doi.org/10.1007/s40999-019-00485-4.

Kitaura, M., and M. Miyajima. 1988. "Quantitative evaluation of damage to buried pipelines induced by soil liquefaction." In *Proc., 9th World Conf. on Earthquake Engineering*, 11–16. Tokyo, Japan: Japan Association for Earthquake Disaster Prevention.

Kosekt, J., O. Matsuo, and Y. Koga. 1997. "Uplift behavior of underground structures caused by liquefaction of surrounding soil during earthquake." *Soils Found.* 37 (1): 97–108. https://doi.org/10.3208/sandf.37.97.

Ling, H. I., Y. Mohri, T. Kawabata, H. Liu, C. Burke, and L. Sun. 2003. "Centrifugal modeling of seismic behavior of large-diameter pipe in liquefiable soil." *J. Geotech. Geoenviron. Eng.* 129 (12): 1092–1101. https://doi.org/10.1061/(asce)1090-0241(2003)129:12(1092).

Ling, H. I., L. Sun, H. Liu, Y. Mohri, and T. Kawabata. 2008. "Finite element analysis of pipe buried in saturated soil deposit subject to earthquake loading." *J. Earthquake Tsunami* 2 (1): 1–17. https://doi.org/10.1142/s1793431108000244.

Liu, J., M. Liu, and Z. Zhu. 2012. "Sand deformation around an uplift plate anchor." *J. Geotech. Geoenviron. Eng.* 138 (6): 728–737. https://doi.org/10.1061/(ASCE)GT.1943-5606.0000633.

Liu, H., and E. Song. 2005. "Seismic response of large underground structures in liquefiable soils subjected to horizontal and vertical earthquake excitations." *Comput. Geotech.* 32 (4): 223–244. https://doi.org/10.1016/j.compgeo.2005.02.002.

Liu, H., and E. Song. 2006. "Working mechanism of cutoff walls in reducing uplift of large underground structures induced by soil liquefaction." *Comput. Geotech.* 33 (4–5): 209–221. https://doi.org/10.1016/j.compgeo.2006.07.002.
Lutenegger, A. J. 2011. "Behavior of multi-helix screw anchors in sand." In *Proc., 14th Pan-American Conf. on Soil Mechanical Geotechnical Engineering*. London: International Society for Soil Mechanics and Geotechnical Engineering (ISSMGE).
Mahmoud, A. O., M. N. Hussien, M. Karray, M. Chekired, C. Bessette, and L. Jinga. 2020. "Mitigation of liquefaction-induced uplift of underground structures." *Comput. Geotech.* 125: 103663. https://doi.org/10.1016/j.compgeo.2020.103663.
Mahmoudi-Mehrizi, M. E., and A. Ghanbari. 2021. "A review of the advancement of helical foundations from 1990–2020 and the barriers to their expansion in developing countries." *J. Eng. Geol.* 14 (5): 37–84.
Mehrzad, B., A. Haddad, and Y. Jafarian. 2016. "Centrifuge and numerical models to investigate liquefaction-induced response of shallow foundations with different contact pressures." *Int. J. Civ. Eng.* 14 (2): 117–131. https://doi.org/10.1007/s40999-016-0014-5.
Mehrzad, B., Y. Jafarian, C. J. Lee, and A. H. Haddad. 2018. "Centrifuge study into the effect of liquefaction extent on permanent settlement and seismic response of shallow foundations." *Soils Found.* 58 (1): 228–240. https://doi.org/10.1016/j.sandf.2017.12.006.
Mele, L., S. Lirer, and A. Flora. 2019. "The effect of densification on Pieve di Cento sands in cyclic simple shear tests." In *Proc., National Conf. Researchers of Geotech. Eng*, edited by F. Calvetti, F. Cotecchia, A. Galli, and C. Jommi, 446–453. Cham, Switzerland: Springer.
Mitsuji, K. 2008. "Numerical simulations for development of liquefaction. Countermeasures by use of partially saturated sand." In *Proc., 14th World Conf. on Earthquake Engineering*. China: China Earthquake Administration.
Miyajima, M., M. Yoshida, and M. Kitaura. 1992. "Small scale tests on countermeasures against liquefaction for pipelines using gravel drain system." In *Proc., 4th Japan–US Workshop on Earthquake Resistant Design of Lifeline Facilities and Countermeasures for Soil Liquefaction*, 381–391. Buffalo, NY: Multidisciplinary Center for Earthquake Engineering Research.
Modoni, G., M. Albano, E. Salvatore, and J. Koseki. 2018. "Effects of compaction on the seismic performance of embankments built with gravel." *Soil Dyn. Earthquake Eng.* 106: 231–242. https://doi.org/10.1016/j.soildyn.2018.01.005.
Mohajerani, A., D. Bosnjak, and D. Bromwich. 2016. "Analysis and design methods of screw piles: A review." *Soils Found.* 56 (1): 115–128. https://doi.org/10.1016/j.sandf.2016.01.009.
Murray, E. J., and J. D. Geddes. 1987. "Uplift of anchor plates in sand." *J. Geotech. Eng.* 113 (3): 202–215. https://doi.org/10.1061/(ASCE)0733-9410(1987)113:3(202).
Nath, S. K., C. Ghatak, A. Biswas, and A. Srivastava. 2022. "Liquefaction susceptibility mapping in West Bengal with emphasis on its Capital City Kolkata under the impact of a few great earthquakes triggered from the Himalaya and Northeast India." *J. Rehabil. Civ. Eng.* 10 (4): 56–96. https://doi.org/10.22075/JRCE.2021.24034.1533.
Olarte, J. C., S. Dashti, A. B. Liel, and B. Paramasivam. 2018. "Effects of drainage control on densification as a liquefaction mitigation technique." *Soil Dyn. Earthquake Eng.* 110: 212–231. https://doi.org/10.1016/j.soildyn.2018.03.018.
Orense, R. P., I. Morimoto, Y. A. Yamamoto, T. Yumiyama, H. Yamamoto, and K. Sugawara. 2003. "Study on wall-type gravel drains as liquefaction countermeasure for underground structures." *Soil Dyn. Earthquake Eng.* 23 (1): 19–39. https://doi.org/10.1016/S0267-7261(02)00152-5.
Otsubo, M., I. Towhata, T. Hayashida, B. Liu, and S. Goto. 2016b. "Shaking table tests on liquefaction mitigation of embedded lifelines by backfilling with recycled materials." *Soils Found.* 56 (3): 365–378. https://doi.org/10.1016/j.sandf.2016.04.004.
Otsubo, M., I. Towhata, T. Hayashida, M. Shimura, T. Uchimura, B. Liu, D. Taeseri, B. Cauvin, and H. Rattez. 2016a. "Shaking table tests on mitigation of liquefaction vulnerability for existing embedded lifelines." *Soils Found.* 56 (3): 348–364. https://doi.org/10.1016/j.sandf.2016.04.003.
Paramasivam, B., S. Dashti, and A. Liel. 2018. "Influence of prefabricated vertical drains on the seismic performance of structures founded on liquefiable soils." *J. Geotech. Geoenviron. Eng.* 144 (10): 04018070. https://doi.org/10.1061/(ASCE)GT.1943-5606.0001950.
Perko, H. A. 2009. *Helical piles: A practical guide to design and installation*. Hoboken, NJ: Wiley.
Sakr, M. 2009. "Performance of helical piles in oil sand." *Can. Geotech. J.* 46 (9): 1046–1061. https://doi.org/10.1139/T09-044.
Sharma, A., and S. Guner. 2020. "System-level modeling methodology for capturing the pile cap, helical pile group, and soil interaction under uplift loads." *Eng. Struct.* 220: 110977. https://doi.org/10.1016/j.engstruct.2020.110977.
Stringer, M., and G. Madabhushi. 2007. "Modelling of liquefaction around tunnels." In *Proc., 4th Int. Conf. Earthquake Geotechnical Engineering*. Dordrecht, Netherlands: Springer.
Sudevan, P. B., A. Boominathan, and S. Banerjee. 2018. "Uplift analysis of an underground structure in a liquefiable soil subjected to dynamic loading." In *Geotechnical Earthquake Engineering and Soil Dynamics V: Numerical Modeling and Soil Structure Interaction*, Geotechnical Special Publication 292, edited by S. J. Brandenberg and M. T. Manzari, 464–472. Reston, VA: ASCE.
Sudevan, P. B., A. Boominathan, and S. Banerjee. 2020a. "Numerical study of liquefaction-induced uplift of underground structure." *Int. J. Geomech.* 20 (2): 06019020. https://doi.org/10.1061/(ASCE)GM.1943-5622.0001578.
Sudevan, P. B., A. Boominathan, and S. Banerjee. 2020b. "Mitigation of liquefaction-induced uplift of underground structures by soil replacement methods." *Geomech. Eng.* 23 (4): 365–379. https://doi.org/10.12989/gae.2020.23.4.365.
Sutherland, H. B. 1988. "Uplift resistance of soils." *Geotechnique* 38 (4): 493–516. https://doi.org/10.1680/geot.1988.38.4.493.
Taeseri, D., J. Laue, M. Otsubo, and I. Towhata. 2016. "New mitigation method for pipeline uplift during seismic event." *Geotech. Res.* 3 (2): 54–64. https://doi.org/10.1680/jgere.16.00002.
Tagaya, K., R. F. Scott, and H. Aboshi. 1988. "Pullout resistance of buried anchor in sand." *Soils Found.* 28 (3): 114–130. https://doi.org/10.3208/sandf1972.28.3_114.
Tanaka, Y., H. Komine, J. I. Tohma, K. Ohtomo, H. Tochigi, H. Abo, and S. Fukuda. 1995. "Area of compaction to prevent uplift by liquefaction." In *Proc., 3rd Int. Conf. on Recent Advances in Geotechnical Earthquake Engineering and Soil Dynamics*, 2–7. Rolla, MO: Civil, Architectural and Environmental Engineering, Univ. of Missouri.
Tobita, T., S. Iai, G. C. Kang, and Y. Konishi. 2009. "Observed damage of wastewater pipelines and estimated manhole uplifts during the 2004 Niigataken Chuetsu, Japan, earthquake." In *Technical Council on Lifeline Earthquake Engineering Con.*, edited by A. K. K. Tang and S. Werner, 1–12. Reston, VA: ASCE.
Tobita, T., G. C. Kang, and S. Iai. 2011. "Centrifuge modeling on manhole uplift in a liquefied trench." *Soils Found.* 51 (6): 1091–1102. https://doi.org/1091-1102.10.3208/sandf.51.1091.
Wang, L., P. Zhang, H. Ding, Y. Tian, and X. Qi. 2020. "The uplift capacity of single-plate helical pile in shallow dense sand including the influence of installation." *Mar. Struct.* 71: 102697. https://doi.org/10.1016/j.marstruc.2019.102697.
White, D. J., C. Y. Cheuk, and M. D. Bolton. 2008. "The uplift resistance of pipes and plate anchors buried in sand." *Geotechnique* 58 (10): 771–779. https://doi.org/10.1680/geot.2008.3692.
Yang, D., E. Naesgaard, P. M. Byrne, K. Adalier, and T. Abdoun. 2004. "Numerical model verification and calibration of George Massey Tunnel using centrifuge models." *Can. Geotech. J.* 41 (5): 921–942. https://doi.org/10.1139/t04-039.
Yasuda, S., and H. Kiku. 2006. "Uplift of sewage manholes and pipes during the 2004 Niigataken-Chuetsu earthquake." *Soils Found.* 46 (6): 885–894. https://doi.org/10.3208/sandf.46.885.
Yegian, M. K., E. Eseller-Bayat, A. S. Alshawabkeh, and S. Ali. 2007. "Induced-partial saturation for liquefaction mitigation: Experimental investigation." *J. Geotech. Geoenviron. Eng.* 133 (4): 372–380. https://doi.org/10.1061/(ASCE)1090-0241(2007)133:4(372).
Yoshimi, Y. 1998. "Simplified design of structures buried in liquefiable soil." *Soils Found.* 38 (1): 235–240. https://doi.org/10.3208/sandf.38.235.
Zheng, G., P. Yang, H. Zhou, W. Zhang, T. Zhang, and S. Ma. 2021. "Numerical modeling of the seismically induced uplift behavior of twin tunnels." *Int. J. Geomech.* 21 (1): 04020240. https://doi.org/10.1061/(ASCE)GM.1943-5622.0001897.